May 24, 2023, Saint-Gallen, Switherland

First steps of the melting of an amorphous polymer through a hot-end of a material extrusion additive manufacturing

Franck Pigeonneau[1], Sarah Marion[2], Lucas Sardo[3] & Thomas Joffre[4]
[1]Mines Paris | PSL Univ. - Centre of Materials Forming, CNRS UMR 7635, Sophia Antipolis, France
[2]Mines Saint-Etienne, Univ Lyon, CNRS UMR 5307 LGF, Centre SMS, Saint-Etienne, France
[3]Sciences Computers Consultants, Saint-Etienne, France
[4]IPC Innovation Plasturgie Composites, Bellignat, France

Material extrusion

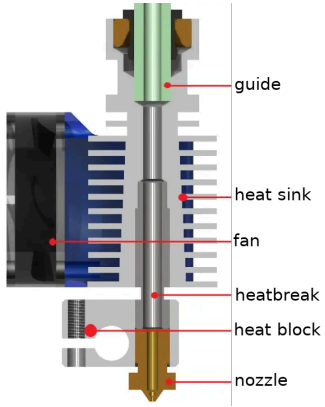

Figure 1: Extruder E3D-V6 according to E3D-online[1].

[1] E3D-online: E3D Help Centre, https://e3d-online.zendesk.com/hc/en-us, 2021.

Material extrusion

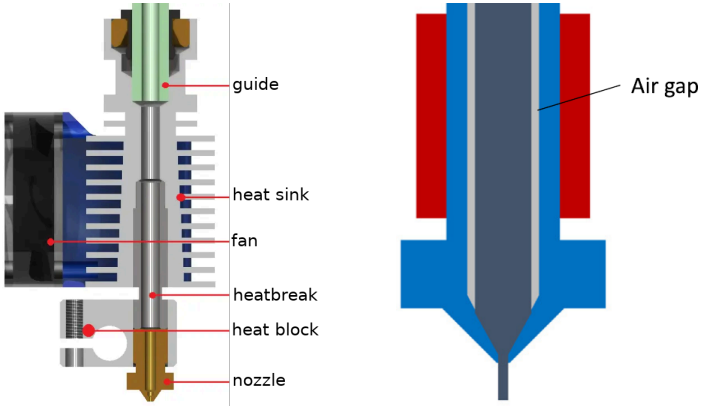

Figure 1: Extruder E3D-V6 according to E3D-online[1] and presence of air gap.

[1] E3D-online: E3D Help Centre (see n. 1).

Material extrusion

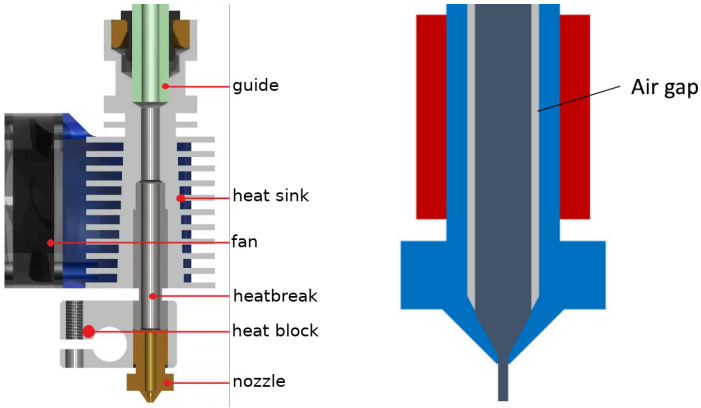

Figure 1: Extruder E3D-V6 according to E3D-online[1].

How does the polymer melt?

[1] E3D-online: E3D Help Centre (see n. 1).

Material extrusion

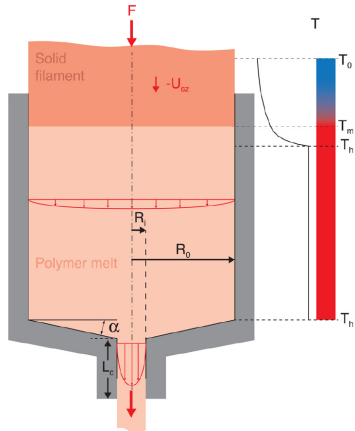

Figure 2: Melting according to Bellini et al.[2].

[2] A. Bellini/S. Güçeri/M. Bertoldi: Liquefier dynamics in fused deposition, in: J. Manuf. Sci. Eng. 126.2 (2004), pp. 237–246.

Material extrusion

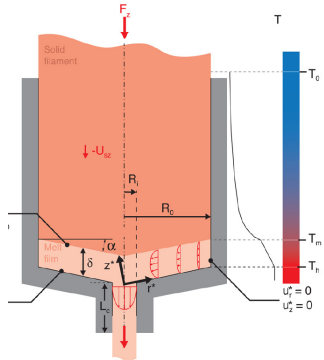

Figure 3: Melting according to Osswald et al.[3].

[3] T. A. Osswald/J. Puentes/J. Kattinger: Fused filament fabrication melting model, in: Addit. Manuf. 22 (2018), pp. 51–59.

Material extrusion

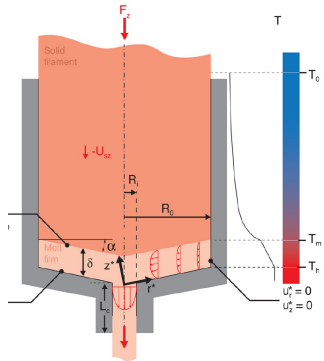

Figure 3: Melting according to Osswald et al.[3].

Numerical computation of the melting of polymer in the extruder

[3] Osswald/Puentes/Kattinger: Fused filament fabrication melting model (see n. 3).

1. Problem statement

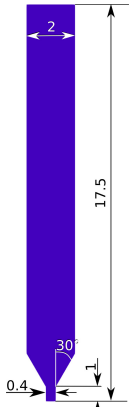

Figure 4: Channel with dimensions (mm) used in the numerical computation.

Main assumptions

- Fluid dynamics & heat transfer are accounted for in the heatblock channel.
- Polymer considered as solid at the entrance of the channel.
- Two-phase dynamics is considered using a single fluid representation.
- Interface between the two phases is assumed sharp and implicitly tracked by a level-set method.
- The two phases are incompressible.
- Polymer viscosity follows a Carreau-Yasuda's law.

1. Problem statement

Table 1: Characteristic variables used in the normalisation.

t	$\mathbf{x}$	$\mathbf{u}$	P	T
$\frac{D}{U}$	D	$U = \frac{4Q}{\pi d^2}$	$\eta_{p,0}\frac{U}{D}$	$\theta = \frac{T-T_0}{T_\infty - T_0}$

$$\eta_p(\dot{\gamma}, T) = \frac{\eta_{p,0} a_T}{[1 + (\lambda a_T \dot{\gamma})^a]^{(1-n)/a}}, \quad (1) \qquad a_T = \exp\left[\frac{E_a}{R}\left(\frac{1}{T} - \frac{1}{T_{\text{ref}}}\right)\right], \quad (2)$$

$$\dot{\gamma} = \sqrt{2\dot{\boldsymbol{\epsilon}} : \dot{\boldsymbol{\epsilon}}}. \quad (3)$$

Table 2: Dimensionless numbers, names, definitions.

Reynolds	capillary	Péclet	Brinkman	Weissenberg
Re	Ca	Pe	Br	Wi
$\frac{\rho_p U D}{\eta_{p,0}}$	$\frac{U\eta_{p,0}}{\gamma}$	$\frac{UD}{a_p}$	$\frac{\eta_{p,0}U^2}{k_p(T_\infty - T_0)}$	$\frac{\lambda U}{D}$

1. Problem statement

Governing equations

$$\boldsymbol{\nabla} \cdot \mathbf{u} = 0, \tag{4}$$

$$\mathrm{Re}\,\rho \frac{D\mathbf{u}}{Dt} = -\boldsymbol{\nabla} P + \boldsymbol{\nabla} \cdot [2\eta(\dot{\gamma}, \theta, \varphi)\dot{\boldsymbol{\epsilon}}] + \mathrm{Ca}^{-1}\,\kappa \|\boldsymbol{\nabla}\varphi\| \delta(\varphi)\mathbf{n}_{\varphi}, \tag{5}$$

$$\mathrm{Pe}\,\rho C_p \frac{D\theta}{Dt} = \boldsymbol{\nabla} \cdot [k\boldsymbol{\nabla}\theta] + \mathrm{Br}\,\eta(\dot{\gamma}, \theta, \varphi)\dot{\gamma}^2, \tag{6}$$

$$\frac{D\varphi}{Dt} = 0. \tag{7}$$

1. Problem statement

Governing equations

$$\boldsymbol{\nabla} \cdot \mathbf{u} = 0, \tag{4}$$

$$\mathrm{Re}\,\rho \frac{D\mathbf{u}}{Dt} = -\boldsymbol{\nabla} P + \boldsymbol{\nabla} \cdot [2\eta(\dot{\gamma}, \theta, \varphi)\dot{\boldsymbol{\epsilon}}] + \mathrm{Ca}^{-1}\,\kappa \|\boldsymbol{\nabla}\varphi\| \delta(\varphi)\mathbf{n}_\varphi, \tag{5}$$

$$\mathrm{Pe}\,\rho C_p \frac{D\theta}{Dt} = \boldsymbol{\nabla} \cdot [k\boldsymbol{\nabla}\theta] + \mathrm{Br}\,\eta(\dot{\gamma}, \theta, \varphi)\dot{\gamma}^2, \tag{6}$$

$$\frac{D\varphi}{Dt} = 0. \tag{7}$$

Surface operators at the interface

$$\mathbf{n}_\varphi = \frac{\boldsymbol{\nabla}\varphi}{\|\boldsymbol{\nabla}\varphi\|}, \tag{8}$$

$$\kappa = -\boldsymbol{\nabla}_S \cdot \mathbf{n}_\varphi. \tag{9}$$

1. Problem statement

Governing equations

$$\boldsymbol{\nabla} \cdot \mathbf{u} = 0, \tag{4}$$

$$\mathrm{Re}\,\rho \frac{D\mathbf{u}}{Dt} = -\boldsymbol{\nabla} P + \boldsymbol{\nabla} \cdot [2\eta(\dot{\gamma}, \theta, \varphi)\dot{\boldsymbol{\epsilon}}] + \mathrm{Ca}^{-1}\,\kappa \|\boldsymbol{\nabla}\varphi\| \delta(\varphi)\mathbf{n}_\varphi, \tag{5}$$

$$\mathrm{Pe}\,\rho C_p \frac{D\theta}{Dt} = \boldsymbol{\nabla} \cdot [k\boldsymbol{\nabla}\theta] + \mathrm{Br}\,\eta(\dot{\gamma}, \theta, \varphi)\dot{\gamma}^2, \tag{6}$$

$$\frac{D\varphi}{Dt} = 0. \tag{7}$$

Surface operators at the interface

$$\mathbf{n}_\varphi = \frac{\boldsymbol{\nabla}\varphi}{\|\boldsymbol{\nabla}\varphi\|}, \tag{8}$$

$$\kappa = -\boldsymbol{\nabla}_S \cdot \mathbf{n}_\varphi. \tag{9}$$

Average properties

$$\rho(\varphi) = H(\varphi) + [1 - H(\varphi)]\,\rho_{\mathrm{air}}, \tag{10}$$

$$\frac{1}{k(\varphi)} = H(\varphi) + \frac{1 - H(\varphi)}{k_{\mathrm{air}}}. \tag{11}$$

1. Problem statement

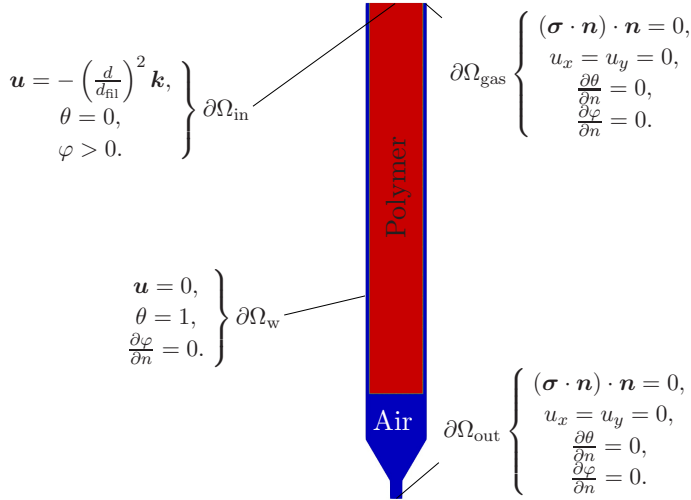

Figure 5: Boundary conditions on the channel with the initial position of the polymer and air.

2. Numerical implementation

- Finite element method using our own C++ library, `CIMLIB_CFD`.
- Implicit Euler scheme is implemented to describe time derivative.
- $\mathbb{P}_1-$bubble$/\mathbb{P}_1$ element to satisfy the inf $-$ sup condition.
- Equations on θ and φ are stabilised using Streamline Upwind/Petrov-Galerkin (SUPG) method.
- Eikonal property of φ, i.e., $\|\boldsymbol{\nabla}\varphi\| = 1$ is conserved using a direct re-initialisation scheme[4].
- An adaptive anisotropic mesh is used[5].

[4] M. Shakoor et al.: An efficient and parallel level set reinitialization method - Application to micromechanics and microstructural evolutions, in: Appl. Math. Modell. 39.23 (2015), pp. 7291–7302.

[5] G. Jannoun et al.: Anisotropic meshing with time-stepping control for unsteady convection-dominated problems, in: Appl. Math. Modell. 39.7 (2015), pp. 1899–1916.

3. Materials and working conditions

Table 3: Parameters used in Carreau-Yasuda and Arrhenius laws for the ABS.

$\eta_{p,0}$	λ	n	a	E_a	T_{ref}
Pa s	s	–	–	kJ mol^{-1}	K
3.04×10^3	3.2×10^{-2}	0.28	0.6	115.06	493.15

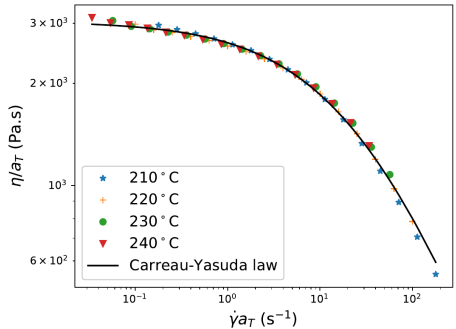

Figure 6: $\eta(\dot{\gamma}, T)/a_T$ vs. $\dot{\gamma}a_T$ for the ABS at 4 T.

3. Materials and working conditions

Table 4: Thermal properties for the ABS[6] and air[7].

ρ	C_p	k
$\mathrm{kg/m^3}$	$\mathrm{J\,kg^{-1}\,K^{-1}}$	$\mathrm{W\,m^{-1}\,K^{-1}}$
ABS		
1150	2100	0.21
Air, $T = T_{\mathrm{ext}}$		
0.701	1034.78	0.0399

[6] M. E. Mackay et al.: The performance of the hot end in a plasticating 3D printer, in: J. Rheol. 61.2 (2017), pp. 229–236.

[7] K. Kadoya/N. Matsunaga/A. Nagashima: Viscosity and Thermal Conductivity of Dry Air in the Gaseous Phase, in: J. Phys. Chem. Ref. Data 14.4 (1985), pp. 947–970.

3. Materials and working conditions

Table 4: Thermal properties for the ABS[6] and air[7].

ρ	C_p	k
$\mathrm{kg/m^3}$	$\mathrm{J\,kg^{-1}\,K^{-1}}$	$\mathrm{W\,m^{-1}\,K^{-1}}$
ABS		
1150	2100	0.21
Air, $T = T_{\mathrm{ext}}$		
0.701	1034.78	0.0399

Table 5: Definitions of working conditions.

Case	U ($\mathrm{m\,min^{-1}}$)	U_{in} ($\mathrm{mm\,s^{-1}}$)	T_0 (°C)	T_∞ (°C)
1	1	0.87		
2	3	2.61	24	230
3	6	5.22		

[6] Mackay et al.: The performance of the hot end in a plasticating 3D printer (see n. 6).

[7] Kadoya/Matsunaga/Nagashima: Viscosity and Thermal Conductivity of Dry Air in the Gaseous Phase (see n. 7).

4. Results

Triple line location and T

U=1 m min^{-1}

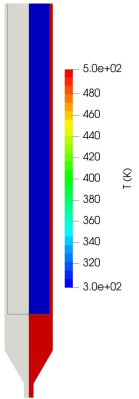

U=3 m min^{-1}

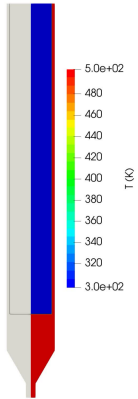

U=6 m min^{-1}

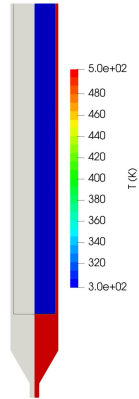

4. Results

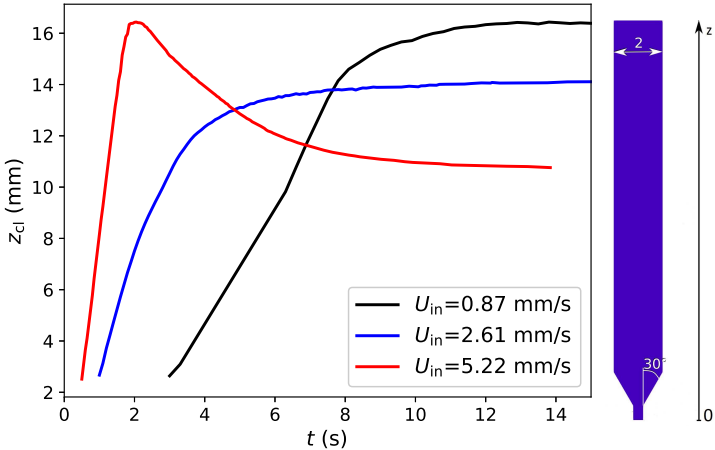

Figure 7: z_{cl} vs. t (s) for the three cases.

4. Results

- The feeding force is numerically evaluated using the Berker's theorem[8]:

Theorem

For a velocity field with no-slip condition on a wall, the tension on the wall is given by

$$\mathbf{T} = \left(P - \frac{4\eta}{3} \boldsymbol{\nabla} \cdot \mathbf{u} \right) \mathbf{n} + 2\eta \mathbf{n} \times \boldsymbol{\omega}, \tag{12}$$

with

$$\boldsymbol{\omega} = \frac{1}{2} \boldsymbol{\nabla} \times \mathbf{u}. \tag{13}$$

Proof.

Corollary of the Stokes theorem. □

- Vorticity is determined using Paraview.

[8] R. Berker: Intégration des équations du mouvement d'un fluide visqueux incompressible, in: Handbuch der Physik, Berlin 1963.

4. Results

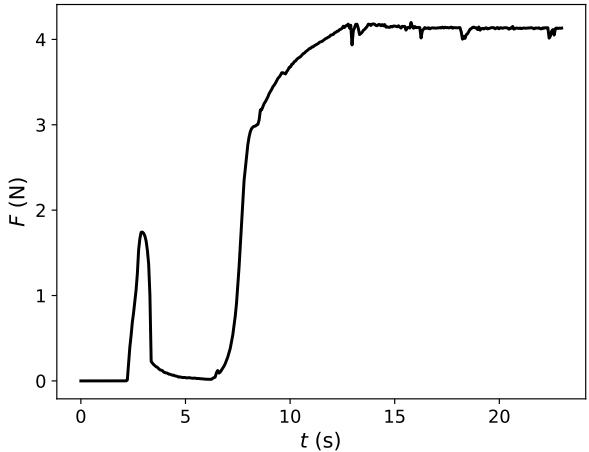

Figure 8: Feeding force vs. t for U=1 m min^{-1}.

4. Results

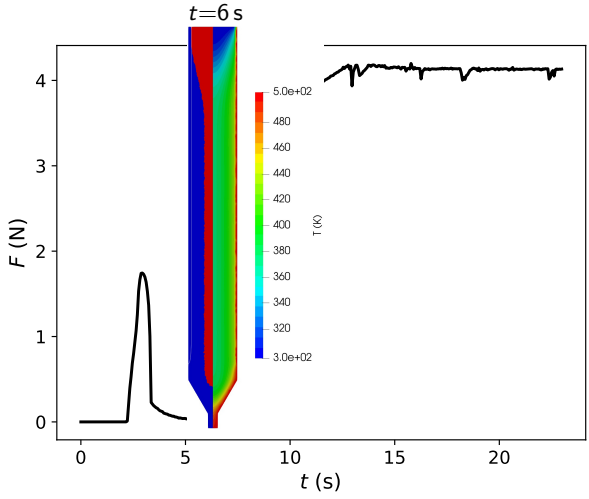

Figure 8: Feeding force vs. t for U=1 m min^{-1}.

4. Results

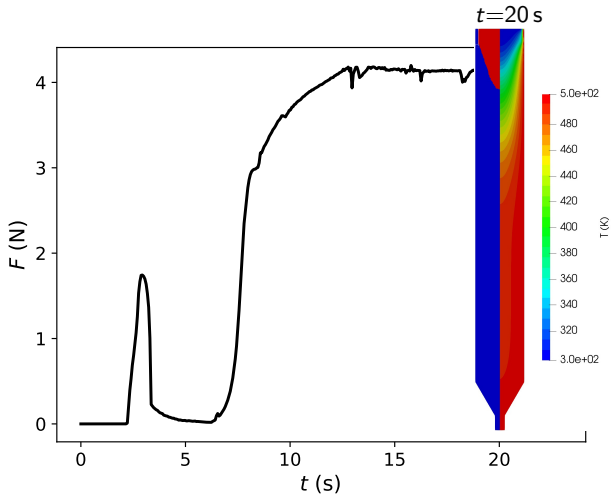

Figure 8: Feeding force vs. t for U=1 m min^{-1}.

4. Results

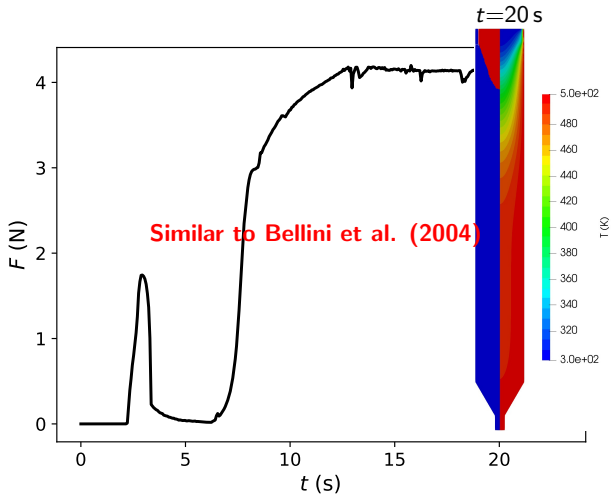

Figure 8: Feeding force vs. t for U=1 m min^{-1}.

4. Results

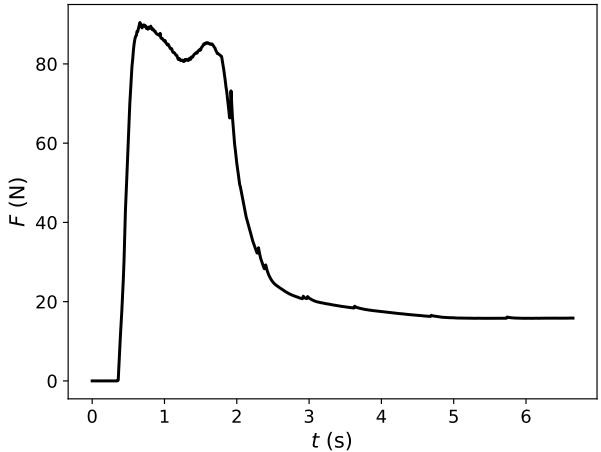

Figure 9: Feeding force vs. t for U=6 m min^{-1}.

4. Results

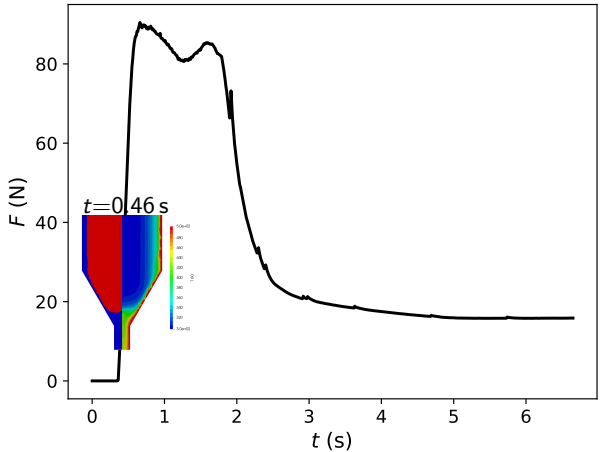

Figure 9: Feeding force vs. t for U=6 m min^{-1}.

4. Results

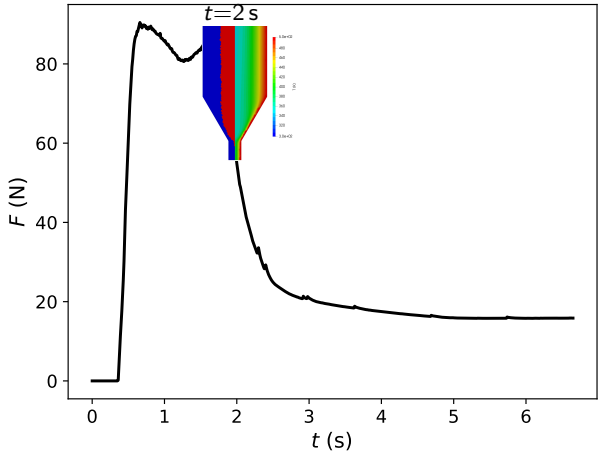

Figure 9: Feeding force vs. t for U=6 m min^{-1}.

4. Results

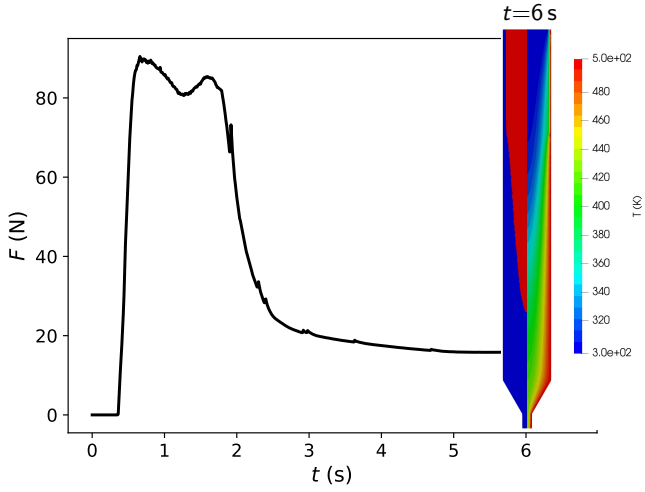

Figure 9: Feeding force vs. t for U=6 m min^{-1}.

4. Results

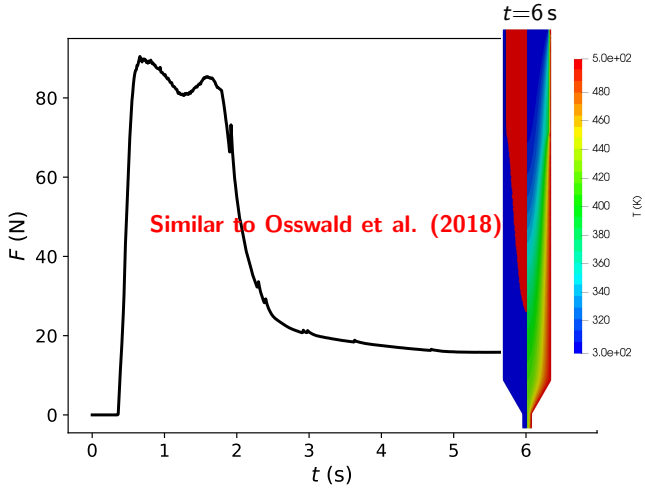

Figure 9: Feeding force vs. t for U=6 m min^{-1}.

4. Results

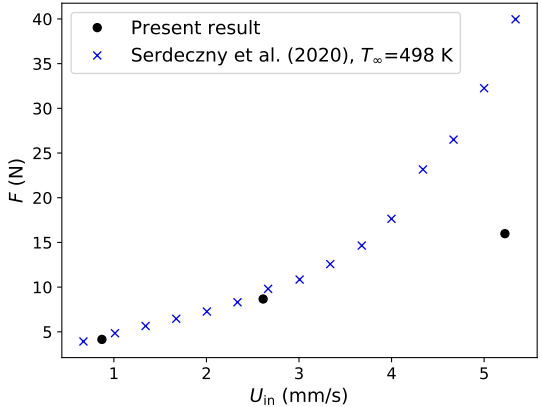

Figure 10: F (N) vs. U_{in} (mm min^{-1}) for T_∞=230 °C and comparison with Serdeczny et al.[9] at T_∞=225 °C.

[9] M. P. Serdeczny et al.: Numerical modeling of the polymer flow through the hot-end in filament-based material extrusion additive manufacturing, in: Addit. Manuf. 36 (2020), p. 101454.

5. Synthesis

- Numerical investigations focus on the melting in a particular extruder (E3D-V6).
- Two-phase flow accurately described using a level-set method.
- Air gap persists at high feeding velocity.
- Dynamics of the rising of the contact line in agreement with Hong et al.[10].
- At small feeding rate, polymer fully melted in agreement with Bellini et al. (2004).
- At large feeding rate, polymer partially melted in agreement with Osswald et al. (2008).
- Details can be found in Marion et al.[11].

[10] Y. Hong et al.: In-situ observation of the extrusion processes of Acrylonitrile Butadiene Styrene and Polylactic Acid for material extrusion additive manufacturing, in: Addit. Manuf. 49 (2022), p. 102507.

[11] S. Marion et al.: First steps of the melting of an amorphous polymer through a hot-end in Fused Filament Fabrication, in: Addif. Manuf. 65 (2023), p. 103435.

Acknowledgements

Work supported by the Carnot Institutes M.I.N.E.S and ingenierie@Lyon through the CARATS project funded by the Programme des Investissements d'Avenir and the Agence Nationale de la Recherche, France

Acknowledgements

Work supported by the Carnot Institutes M.I.N.E.S and ingenierie@Lyon through the CARATS project funded by the Programme des Investissements d'Avenir and the Agence Nationale de la Recherche, France

Sarah Marion

Lucas Sardo

Thomas Joffre

Acknowledgements

Work supported by the Carnot Institutes M.I.N.E.S and ingenierie@Lyon through the CARATS project funded by the Programme des Investissements d'Avenir and the Agence Nationale de la Recherche, France

Sarah Marion

Lucas Sardo

Thomas Joffre

Thank you for your attention!

Contact: franck.pigeonneau@minesparis.psl.eu